AIAA 96-4136
Response Surface Approximations for Pitching Moment, Including Pitch-Up, in the MDO Design of an HSCT

P.J. Crisafulli, M. Kaufman, A.A. Giunta,
W.H. Mason, B. Grossman and L.T. Watson
Virginia Polytechnic Institute and
State University, Blacksburg, VA 24061

and

R.T. Haftka
University of Florida
Gainesville, FL 32611-6250

6th AIAA/NASA/ISSMO
Symposium on Multidisciplinary Analysis and Optimization
September 4-6, 1996 / Bellevue, WA

RESPONSE SURFACE APPROXIMATIONS FOR PITCHING MOMENT INCLUDING PITCH-UP IN THE MDO DESIGN OF AN HSCT

Paul Crisafulli,* Matthew Kaufman,* Anthony A. Giunta,*
William H. Mason,† Bernard Grossman,‡ and Layne T. Watson§
Multidisciplinary Analysis and Design (MAD) Center for Advanced Vehicles
Virginia Polytechnic Institute and State University, Mail Stop 0203, Blacksburg, Virginia 24061
and
Raphael T. Haftka¶
Dept. of Aerospace Engineering, Mechanics and Engineering Science, Univ. of Florida
Gainesville, Florida 32611-6250

Abstract

A procedure for incorporating key non-linear aerodynamic characteristics into the design optimization of a high-speed civil transport has been developed. Previously, planforms which were likely to exhibit pitch-up in low speed flight could not be included directly in the design process. Using response surface methodology, polynomial approximations to the results obtained from a computationally expensive estimation method were developed by analyzing a set of statistically selected wing shapes. These response surface models were then used during the optimization process to approximate the effects of wing planform changes on pitch-up. In addition, response surface approximations were used to model the effect of horizontal tail size and wing flaps on the performance of the aircraft. Optimization studies of the high-speed civil transport were done with and without the response surfaces. The results of this study provide insight into the influence of both nonlinear aerodynamics and high lift aerodynamics on the design of a high-speed civil transport.

List of Symbols

α	angle of attack
α_B	pitch-up angle of attack
ac	aerodynamic center
cg	center of gravity
C_L	lift coefficient
$C_{L\alpha}$	lift curve slope, $\partial C_L/\partial\alpha$
$C_{L\delta e}$	rate of change in lift with elevator deflection, $\partial C_L/\partial\delta e$
$C_{L\delta f}$	rate of change in lift with flap deflection, $\partial C_L/\partial\delta f$
C_M	pitching moment coefficient
$C_{M\alpha}$	rate of change in pitching moment with angle of attack, $\partial C_M/\partial\alpha$
$C_{M\alpha,1}$	$\partial C_M/\partial\alpha$ before pitch-up
$C_{M\alpha,2}$	$\partial C_M/\partial\alpha$ after pitch-up
C_{Mo}	zero lift pitching moment coefficient
$C_{M\delta e}$	rate of change in pitching moment with elevator deflection, $\partial C_M/\partial\delta e$
$C_{M\delta f}$	rate of in pitching moment with flap deflection, $\partial C_M/\partial\delta f$
δe	elevator deflection, positive downward
δf	flap deflection, positive downward
$\Delta C_{M\delta e}$	increment in pitching moment at a given elevator deflection, $(\partial C_m/\partial\delta_e)\cdot\delta_e$
$\Delta C_{M\delta f}$	increment in pitching moment at a particular flap deflection, $(\partial C_M/\partial\delta_f)\cdot\delta_f$
$\Delta C_{L\delta f}$	increment in lift at a particular flap deflection, $(\partial C_L/\partial\delta_f)\cdot\delta_f$
R^2	coefficient of multiple determination[19]

Acronyms

APE	Aerodynamic Pitch-up Estimation
BFL	Balanced Field Length
CCD	Central Composite Design
CFD	Computational Fluid Dynamics
HSCT	High-Speed Civil Transport
LE	leading-edge
MDO	Multidisciplinary Design Optimization
RS	Response Surface
RSM	Response Surface Methodology
TOGW	Take Off Gross Weight
TE	trailing-edge

* Research Assistant, Dept. of Aerospace & Ocean Eng., Virginia Tech, Blacksburg, VA 24061, Student Member AIAA
† Professor, Dept. of Aerospace & Ocean Eng., Virginia Tech, Blacksburg, VA, 24061, Associate Fellow AIAA
‡ Professor & Dept. Head, Dept. of Aerospace & Ocean Eng., Virginia Tech, Blacksburg, VA, 24061, Associate Fellow AIAA
§ Professor, Depts. of Computer Science and Mathematics, Virginia Tech, Blacksburg, VA, 24061
¶ Professor, Dept. of Aerospace Engineering, Mechanics & Engineering Science, University of Florida, Gainesville, FL., Associate Fellow AIAA

1. Introduction

The use of optimization methods in the design of aerospace vehicles is often limited due to the need to use computationally expensive design tools such as Computational Fluid Dynamics (CFD), where a single design point analysis may take many CPU hours and thousands of analyses are needed during a single optimization cycle. In addition, the results often contain small 'wiggles' as a function of the design variables due to the presence of numerical noise, and this affects convergence and lengthens the optimization process. To obtain an optimal aircraft configuration within a reasonable amount of time, algebraic relations or computationally inexpensive models, with a compromise in accuracy, have been used to shorten the optimization cycle in aircraft design programs such as FLOPS[1] and ACSYNT[2]. Another technique is to use a variable complexity modeling approach which involves combining computationally expensive models with simple and computationally inexpensive models. This technique has been previously applied to the aerodynamic-structural optimization of the High-Speed Civil Transport (HSCT)[3,4]. An additional approach is to replace computationally expensive analysis tools with a statistical technique, called response surface methodology, in the actual optimization process. Response surface methodology approximates the response of a computationally expensive analysis tool with a low-order polynomial by examining the response of a set of statistically selected numerical experiments. The result is an extremely fast function evaluation, which not only shortens the optimization process but also filters out any numerical noise generated by the analysis tools. Without numerical noise to create artificial local minima and inhibit optimization, an optimal design is much easier to obtain. The response surface approach has been applied to the wing structural optimization of the HSCT[5] and to the aerodynamic design of the wing of an HSCT[6].

In this study, the integration of a key non-linear aerodynamic characteristic (pitch-up) into the design optimization of a HSCT is addressed using response surface approximations. In previous studies[3-5], variable complexity modeling was used to calculate the linear aerodynamic relationship between the pitching moment and the angle of attack of an HSCT configuration. However, these studies did not include the aerodynamic pitch-up which occurs at low speeds due to non-linear aerodynamic effects related to wing planforms typically proposed for supersonic cruise transports. With the use of the Aerodynamic Pitch-up Estimation (APE) method developed by Benoliel and Mason[7], a means of estimating aerodynamic characteristics and pitch-up of high-speed aircraft wings is now available and can be used during the design optimization.

Optimizations of the HSCT were completed with and without response surface models. The response surface models were used during the optimization to integrate a simple approximation of the aerodynamic characteristics and pitch-up as predicted by the APE method instead of using the APE method itself, where a single analysis may take minutes and thousands of analyses are needed in a single optimization cycle. Another benefit is to smooth out the small-scale noise generated by the APE, which is a problem for the derivative-based optimization method used in this study.

Section 2 is a review of the multidisciplinary design optimization efforts for a high-speed civil transport at Virginia Tech. Pitch-up and the APE method are described in Section 3. Section 4 describes the nonlinear pitching moment and flap effect models. Response surface methodology and its use within optimization is introduced in Section 5. Section 6 applies the response surface methodology to the results of the APE method. Section 7 presents the results of the optimizations of an HSCT with and without the response surface models. Finally, Section 8 presents the conclusions of this study.

2. HSCT Design Optimization

The design problem studied extensively at Virginia Tech is to minimize the takeoff gross weight of a 250 passenger HSCT with a range of 5,500 nautical miles and a cruise speed of Mach 2.4. A design code has been developed which includes conceptual-level and preliminary-level tools which estimate the subsonic and supersonic aerodynamics, takeoff and landing performance, mission performance, propulsion, and weights. The HSCT is defined by 29 variables which include the planform shape and thickness distribution of the wing, the area ruling of the fuselage, engine nacelle locations and size, tail sizes, the cruise trajectory, and the amount of fuel to be carried. The configuration is analyzed and then optimized by evaluating constraints on the geometry, performance, and aerodynamics using the conceptual-level and preliminary-level tools. An optimized HSCT configuration will have the minimum TOGW which satisfies all the constraints on the problem.

Twenty-nine design variables are used to describe the HSCT design problem, and are listed in Table 1. The wing planform is specified using eight design variables, which include the wing root chord, locations of the wing leading-edge and trailing-edge break points, *x*-location of the leading-edge of the wing tip, wing tip chord, and wing semi-span, as shown in Figure 1. The airfoil sections (one span station is shown in Fig. 1) are de-

scribed by five design variables, which include the constant chordwise location of maximum thickness and airfoil leading-edge radius parameter, and the maximum wing thickness at the wing root, leading-edge break, and tip. The fuselage is assumed to be axisymmetric and is area ruled using eight variables which include the axial positions and radii of four fuselage restraint locations. Two design variables position the nacelles spanwise along the trailing-edge of the wing. There are three mission-related design variables. They include the fuel weight, initial supersonic cruise altitude, and constant cruise/climb rate. The horizontal tail and vertical tail areas are described using two variables. These control surfaces are trapezoidal planforms, where the aspect ratio, taper ratio, and quarter chord sweep are fixed. The final design variable specifies the maximum sea level thrust per engine.

Table 1. Design variables.

#	Baseline Value	Description
1	181.5	Wing root chord (ft)
2	155.9	LE break, *x* (ft)
3	49.2	LE break, *y* (ft)
4	181.6	TE break, *x* (ft)
5	64.2	TE break, *y* (ft)
6	169.6	LE of wing tip, *x* (ft)
7	7.0	Tip chord (ft)
8	75.9	Wing semi-span (ft)
9	0.4	Chordwise loc. of max *t/c*
10	3.7	Airfoil LE radius param., r_t
11	2.6	Airfoil *t/c* at root (%)
12	2.2	Airfoil *t/c* at LE break (%)
13	1.8	Airfoil *t/c* at tip (%)
14	2.2	Fuselage restraint 1, *x* (ft)
15	1.1	Fuselage restraint 1, *r* (ft)
16	12.2	Fuselage restraint 2, *x* (ft)
17	3.5	Fuselage restraint 2, *r* (ft)
18	132.5	Fuselage restraint 3, *x* (ft)
19	5.3	Fuselage restraint 3, *r* (ft)
20	248.7	Fuselage restraint 4, *x* (ft)
21	4.6	Fuselage restraint 4, *r* (ft)
22	26.2	Nacelle 1, *y* (ft)
23	32.4	Nacelle 2, *y* (ft)
24	322,617	Mission fuel (lbs)
25	64,794	Starting cruise altitude (ft)
26	33.9	Cruise climb rate (ft/min)
27	697.9	Vertical tail area (sq ft)
28	713.1	Horizontal tail area (sq ft)
29	55,465	Max sea level thrust per engine (lbs)

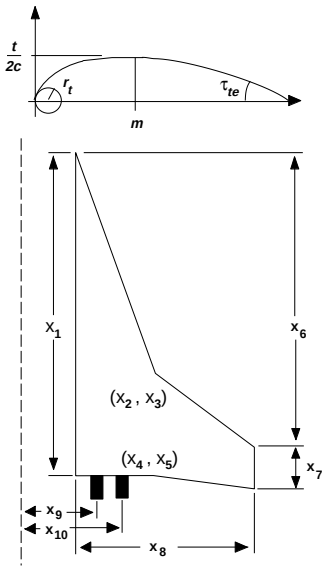

Figure 1. Airfoil section and wing planform with design variables.

A complete design optimization is comprised of a sequence of optimization cycles using sixty-nine constraints (Table 2), which include geometry, performance, and aerodynamic constraints on the design of the HSCT. These constraints are discussed in detail in References 4 and 8. During the optimization, the optimizer (NEWSUMT-A[9]) is used to identify an optimal aircraft design which satisfies all sixty-nine constraints with a minimum TOGW. To shorten the entire optimization, variable-complexity modeling is used to scale the results of simple analyses to the results of computationally expensive "exact" analysis methods at the beginning each optimization cycle. These scale factors are carried through the optimization cycle with an added benefit of performing thousands of computationally inexpensive calculations, instead of time-consuming exact calculations, to predict an improved design. At the beginning of the next cycle, the design is evaluated with the exact analysis methods and new scale factors are calculated. This process continues until the design is converged or changes only slightly from cycle to cycle. More details of the variable complexity modeling are in Reference 4. A typical optimization is completed within 25 to 50 cycles using NEWSUMT-A. A typical optimization cycle takes approximately 10 minutes to complete on an SGI Power Challenge workstation with an R-8000 CPU.

Table 2. Optimization constraints.

#	Geometric Constraints
1	Fuel volume ≤ 50% wing volume
2	Wing tip spike-shape prevention
3-20	Wing chord ≥ 7.0 ft
21	LE break ≤ wing semi-span
22	TE break ≤ wing semi-span
23	Root $t/c \geq 1.5\%$
24	LE break $t/c \geq 1.5\%$
25	TE break $t/c \geq 1.5\%$
26-30	Fuselage restraints, x
31	Nacelle 1 ≥ side-of-body
32	Nacelle 1 ≤ nacelle 2
33	Nacelle 2 ≤ wing semi-span
34	No neg. TE sweep inboard TE break
#	Aero. and Performance Constraints
35	Range ≥ 5,500 n.mi.
36	Landing angle-of-attack ≤ 12°
37	Landing $C_L \leq 1.0$
38-56	Landing section $C_l \leq 2.0$
57-59	No engine scrape at landing w/ 5° bank
60-61	No wing scrape at landing with 5° bank
62-63	Limit aileron/rudder to 22.5° and bank to 5° during 20 knot crosswind landing
64	Tail deflect. during approach ≤ 22.5°
65	Takeoff rotation ≤ 5 seconds
66	Engine-out limit with vert. tail design
67	Balanced field length ≤ 11,000 ft
68-69	Required engine thrust ≤ avail. thrust

2.1 Takeoff and Landing Performance

Three constraints on takeoff and landing performance require pitching moment information and currently have a major effect on the horizontal tail size. The take-off constraints include a balanced field length requirement of 11,000 feet and a rotation time to lift-off attitude constraint of less than 5 seconds. For approach trim, the aircraft must trim with a tail deflection of less than 22.5 degrees. These constraints were added to the design code by MacMillin, *et al* [8].

For both the takeoff and landing constraints, the subsonic aerodynamic pitching moment is estimated using two levels of modeling. The detailed calculations for the subsonic lift curve slope and pitching moment curve slope are performed using a vortex-lattice code developed by Hutchison which is discussed in detail in Reference 10. The simple approximation for the pitching moment curve slope is an empirical algebraic relation from the U.S.A.F. Stability and Control DATCOM[11]. In this analysis we neglect the wing camber contribution to C_{Mo} as being small compared to the trailing flap effects.

Takeoff performance is evaluated by integrating the equations of motion during the ground run, rotation, and climb out phases of takeoff. The sum of the horizontal distance covered by the airplane during these three segments is the takeoff field length. The longest distance required for takeoff occurs when an engine fails at a certain critical speed at which time the pilot can decide to abort the takeoff and safely brake to a stop or to continue the takeoff. This distance is known as the balanced field length or FAR takeoff distance.

During the evaluation of the takeoff requirements, lift and moment flap effects are added to the aerodynamics of the airplane. High-lift devices are important for low speed operation of the HSCT[12]. If high-lift devices are ignored, supersonic efficiency is compromised to satisfy low-speed performance requirements such as the takeoff balanced field length. Ground effect and drag due to the landing gear and a windmilling engine are also included within the calculations and are discussed in detail in Reference 8.

The takeoff requirements are calculated with an all-moving horizontal tail deflected -20°, leading-edge flaps deflected 10°, and trailing-edge flaps deflected 20°. The longitudinal control derivatives with respect to horizontal tail deflection ($C_{L\,\delta e}$,$C_{M\delta e}$) are calculated using a vortex lattice code developed by J. Kay[13]. In order to save computational effort, the control derivatives are calculated only every five optimization cycles and are scaled using variable complexity within each optimization cycle. The longitudinal control derivatives with respect to flap deflection ($C_{L\,\delta f}$, $C_{M\delta f}$) were picked based upon investigation of the aerodynamics of AST-105-1 configurations[14] and other proposed HSCT designs[7]. These derivatives were originally fixed throughout the optimization as:

$$C_{L\,\delta f} = 0.2508/\text{rad}$$
$$C_{M\delta f} = -\,0.0550/\text{rad}$$

In this paper we will extend the analysis to allow these values to vary as the wing planform changes.

The aircraft is required to rotate to lift-off in under 5 seconds. If takeoff rotation takes too much time, it will greatly increase the takeoff distance. This requirement was determined by MacMillin, *et al* [8] before the balanced field length constraint was added to our code. After investigating typical rotation times for large aircraft, 5 seconds was adopted as a reasonable assumption. This constraint is active in most of our optimizations. Subsequent studies in Ref. 8 found that this value is slightly less than the rotation time that occurs when it is not used as a constraint. Typical values that occur without the constraint are around 5.6 to 6.4 seconds, and a slightly lighter aircraft results.

The aircraft must be able to be trimmed at an angle of attack well above operating procedures. In

addition, there should be extra control deflection available to allow for pitch control. We require that the tail deflection to trim is less than 22.5 degrees at a landing speed of 145 knots and an altitude of 5000 ft. The tail deflection required to trim the aircraft is determined by calculating the pitching moment about the aircraft center of gravity generated by the lift, pitching moment, drag, thrust, and weight. The tail deflection to trim is then found by calculating the tail deflection needed to trim the pitching moment The approach trim analysis currently neglects the effects of flaps.

3. Pitch-Up and the APE Method

Low aspect ratio, highly-swept cranked delta wings are typically proposed for high-speed civil transports[15]. These planforms are chosen due to the low drag benefits of the highly swept inboard leading-edges. However, this leads to poor low-speed aerodynamic characteristics. A lower sweep outboard section is used to compensate for this deficiency, improving the low speed lift/drag ratio and increasing the lift curve slope. However, at low speeds these wings are susceptible to pitch-up at modest angles-of-attack (as low as 5°) due to non-linear aerodynamic effects, which include leading-edge vortex flow, outer wing stall, and vortex breakdown[7].

Pitch-up is defined as an abrupt change in the slope of the pitching moment curve with respect to the angle-of-attack ($C_{M\alpha}$) such that the slope of the curve after the pitch-up angle-of-attack is increased. The magnitude of the change in slope of the curve and the pitch-up angle-of-attack vary depending on the aircraft configuration. As identified in a study by Benoliel and Mason[7], pitch-up is a result of the forces generated by the leading-edge vortex inboard, together with flow separation and vortex breakdown on the outer portion of the wing. The strong effects of the leading-edge vortex, and the loss of lift on the outboard wing sections due to flow separation, causes the center-of-pressure to move forward, producing the pitch-up behavior. This behavior has yet to be simulated in a complete CFD analysis of an HSCT-class wing undergoing pitch-up at low speed. The APE method described next is a way to estimate this behavior.

To estimate the pitch-up of cranked delta and arrow wing planforms, Benoliel and Mason[7] performed a study on planforms that exhibited pitch-up during experimental investigations. Using a vortex-lattice-type method, *Aero2s*[16], section lift coefficients were plotted for each spanwise station at angles of attack near the pitch-up regime for a variety of planforms. It was determined from this study that an equivalent 2-D section lift coefficient limit could be used to model separated flow on the outboard wing panel. Once this 2-D lift coefficient is exceeded, the total aircraft lift and pitching moment is corrected to include the loss of lift on the outboard wing panel. The resulting Aerodynamic Pitch-up Estimation (APE) method is a computationally inexpensive means of estimating the onset of non-linear aerodynamic characteristics and pitch-up of cranked arrow wings (although still too expensive to be included directly within an optimization).

A comparison of the APE method, *Aero2s*, and wind tunnel data for a cambered and twisted cranked arrow wing tested by Yip and Parlett[17] is presented in Figure 2. The results of the APE method, shown with a solid line, is in good agreement with the experimental data and estimates pitch-up of the configuration fairly well. The pitch break occurs at an angle-of-attack of about 6° at a lift coefficient of about 0.24. Many other comparisons were presented by Benoliel and Mason.

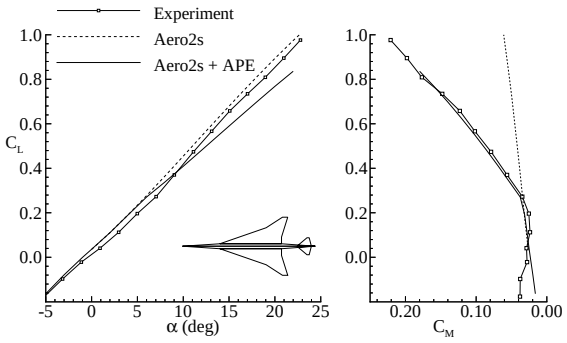

Figure 2. Comparison of lift and pitching moment estimation methods for a 71°/57° swept cambered and twisted wing (δ_{tail} = 0°). (Ref. 7).

4. Nonlinear Pitching Moment Model and Flap Effect Model

In this section, the nonlinear pitching moment and the lift and moment flap effect models are described. The nonlinear pitching moment model is used during the calculation of the takeoff and landing constraints. The flap effect model is only used during the takeoff analysis, since we are currently neglecting flaps within the approach analysis.

The nonlinear pitching moment model is shown in Figure 3 together with results computed by the APE method. The difference between a linear relationship in pitching moment with angle-of-attack and the nonlinear pitching moment model is that the slope of the pitching moment curve changes after the pitch-up angle-of-attack. After examination of typical aerodynamic pitch-up characteristics, and trying several other approaches, we adopted a piecewise linear model. As shown in the figure, three parameters describe the nonlinear behavior with angle of attack. These include the

slope before pitch-up ($C_{M\alpha,1}$), the pitch-up angle-of-attack (α_B), and the slope after pitch-up ($C_{M\alpha,2}$). The pitching moment model also includes a contribution due to tail deflection ($\Delta C_{M\delta e}$) and flap deflection ($\Delta C_{M\delta f}$). The pitching moment at zero angle-of-attack (C_{mo}) is zero.

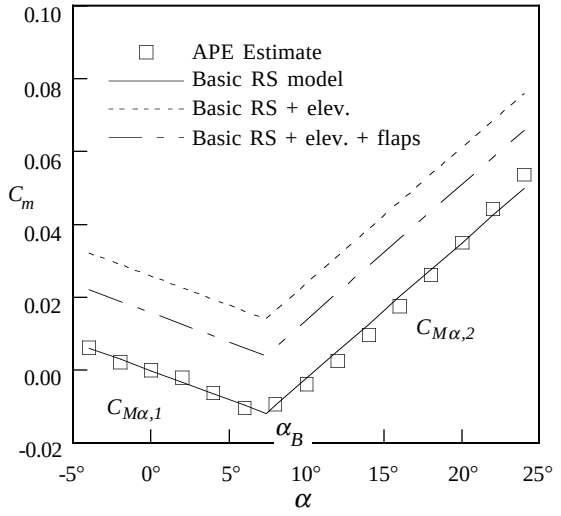

Figure 3. Piecewise linear response surface for pitching moment compared to the APE estimate, and including elevator and flap effects.

The lift and moment flap effect model includes an increment in lift due to flap deflection ($\Delta C_{L\,\delta f}$) and an increment in pitching moment due to flap deflection ($\Delta C_{M\delta f}$), where $\Delta C_{M\delta f}$ is contained within the nonlinear pitching moment model. In the baseline method these values are fixed throughout the optimization at an approximate value based on investigation of HSCT-class aircraft. In this work an improved model is needed to calculate more accurate values and to include effects of changes in the aircraft geometry.

The increments in lift and moment due to flap deflection ($\Delta C_{M\delta f}$, $\Delta C_{L\,\delta f}$) are calculated as average values over the entire angle-of-attack range. As shown in Fig. 4 from experimental data, the flap effectiveness for the pitching moment is fairly linear throughout the angle-of-attack range. However, the flap effectiveness for the lift is not quite linear. The effectiveness decreases with increasing angle of attack. For this study, it was assumed that the flap effectiveness for both the lift and pitching moment are linear to simplify the problem. The size of the leading-edge and trailing-edge flaps are modeled as shown in Fig. 5.

Two separate analyses by *Aero2s* and the APE method are used to calculate the six parameters ($C_{M\alpha,1}$, α_B, $C_{M\alpha,2}$, $\Delta C_{M\delta e}$, $\Delta C_{M\delta f}$, $\Delta C_{L\,\delta f}$) at Mach 0.2 and sea level. For both analyses, *Aero2s* and the APE method require information on the wing and flap geometry, horizontal tail geometry, and the deflections of the tail, leading-edge, and trailing-edge flaps. The first analysis deflects the horizontal tail and a linear least squares fit through the resulting pitching moment data is used to calculate $C_{M\alpha,1}$, α_B, $C_{M\alpha,2}$, and $\Delta C_{M\delta f}$. A second analysis deflects the horizontal tail, leading-edge flaps, and trailing-edge flaps to calculate the average values of the increment in lift and pitching moment due to flap deflection ($\Delta C_{M\delta f}$, $\Delta C_{L\,\delta f}$). Each analysis takes approximately 2 minutes to complete for a single aircraft design.

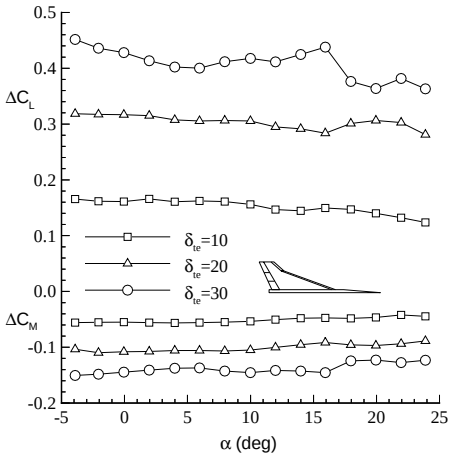

Figure 4. Increments in lift and pitching moment for various trailing-edge flap deflections for a 70°/48.8° sweep flat cranked arrow wing (Ref. 18).

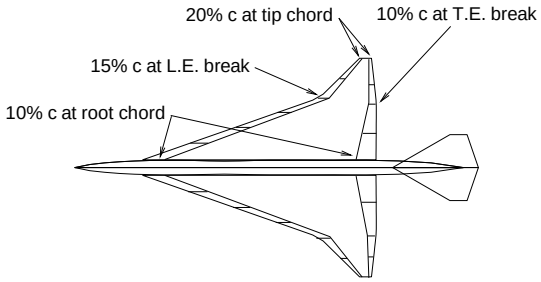

Figure 5. Leading-edge and trailing-edge flaps.

Since each analysis takes approximately 2 minutes, and thousands will be required, it will be inefficient to directly connect *Aero2s* and the APE method to the optimization. Pitching moment and flap effect information is needed whenever the takeoff and approach constraints are calculated for a given aircraft configuration. In addition, the optimizer evaluates many different designs in order to choose a design with a minimum TOGW which satisfies all of the constraints. As a result, the optimization would take too long to find an optimal

solution. Therefore, another method is needed to approximate the results ($C_{M\alpha,1}$, α_B, $C_{M\alpha,2}$, $\Delta C_{M\delta e}$, $\Delta C_{M\delta f}$, $\Delta C_{L\,\delta f}$) from *Aero2s* and the APE method. Response surface methodology will be used for this purpose.

5. Response Surface Methods

In this section, response surface methodology and its use within optimization is briefly discussed. Response surface methods will be used to approximate the pitch-up and flap effect parameters ($C_{M\alpha,1}$, α_B, $C_{M\alpha,2}$, $\Delta C_{M\delta e}$, $\Delta C_{M\delta f}$, $\Delta C_{L\,\delta f}$) calculated by *Aero2s* and the APE method. These parameters will be used within the optimization via the nonlinear pitching moment and the lift and moment flap effect models.

5.1 Response Surfaces

Response surface methodology (RSM) is a technique in which empirical models are developed to approximate an unknown function of a set of variables. Based on statistical and design of experiments theory[19], the empirical model known as the response surface model is constructed by performing a series of numerical experiments and then observing the responses from those experiments. In most cases, the response surface model is a low order polynomial such as a linear or quadratic function of the variables of interest. For example, a second order response surface model for n variables has the form

$$y = c_0 + \sum_{1\le i\le n} c_i x_i + \sum_{1\le i\le j\le n} c_{ij} x_i x_j ,$$

where the x_i are the variables, the c_i are the polynomial coefficients, and y is the predicted response. For n variables, there are $k = (n + 1)(n + 2)/2$ coefficients in the quadratic polynomial. The polynomial coefficients are typically estimated by a least squares fit to the data obtained from the experiments (here they are computer runs). At least $p \ge k$ experiments (analysis runs) are needed to estimate the unknown coefficients. The final result is a regression curve or surface which approximates the response of an unknown function of a set of variables.

5.2 Response Surface Generation

The first step in generating a response surface model is to determine a set of relevant variables within the problem of interest and to construct a design space by determining the minimum and maximum value of each variable. The second step is to determine an appropriate procedure which selects the number of experiments and the combination of variables within each experiment. Typical design of experiment approaches include factorial and central composite designs[20]. In the factorial design, each variable is assigned a certain number of levels or discretized values. For a three-level factorial design, each variable is assigned a minimum, maximum, and midpoint value and 3^n experiments (or design points with a particular set of variables) are generated. A three-level, three variable factorial design is presented in Figure 6 where 27 design points are shown.

If the problem consists of a large number of variables and 3^n experiments are too many to evaluate, the number of experiments can be reduced using a central composite design. In this point selection scheme, each variable is assigned an extreme minimum and maximum value yielding 2^n experiments. In addition, $2n$ experiments are generated by assigning a single variable at a time to its minimum and maximum value multiplied by a scaling factor and keeping the rest of the variables at their midpoint value. The final experiment consists of the midpoint or center design. A three variable central composite design is presented in Fig. 7 where 15 design points are shown.

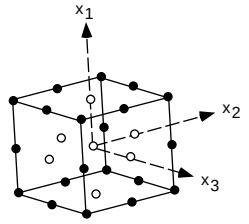

Figure 6. A three-level, three variable factorial design (27 points).

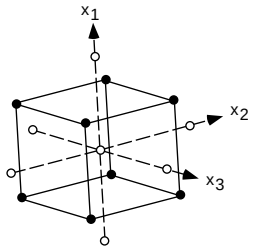

Figure 7. A three variable central composite design (15 points).

If the number of experiments is still too large to evaluate, then the D-optimality criterion[21] can be used to choose a smaller number of points, where the number of experiments is at least the number of coefficients in the response surface model. D-optimality has also been shown to be useful in selecting experiments within irregularly shaped design spaces[6,22]. In most problems, irregularly shaped design spaces are developed by constraining certain portions of the design space due to the nature of the problem.

The final step in the response surface model generation is to evaluate the response at each experimental point. Using the data obtained from these evaluations, a least squares method is used to determine the coefficients of the response surface model. The response surface model is then evaluated by observing how well it approximates the true function or response. This is done by calculating the coefficient of multiple determination,[19] R^2, of the least squares fit. The R^2 value is the square of the correlation between the actual and predicted response. This value estimates the proportion of the variation in the response around the mean that can be attributed to the response surface model rather than to random error (or numerical noise in computational experiments). It is also the square of the correlation between the actual and predicted response. A value of 1.0 indicates a perfect fit (errors are all zero) of the model to the data points.

5.3 Response Surface Models Within Optimization

Response surfaces are used in derivative-based optimization to counteract the adverse affects of numerical noise by creating smooth, polynomial models for the noisy results. Without numerical noise to inhibit optimization, a globally optimal design may be found. Response surface models also have the added benefit of being extremely inexpensive to evaluate during optimization. Therefore, RSM is used to approximate the results obtained from computationally expensive analyses, even though the expensive analyses may not produce numerical noise.

Figure 8 diagrams the procedure used to incorporate response surface models into the optimization process. A set of design variables which are affected by the particular problem are selected and the boundaries of the feasible design space are determined around a baseline or initial HSCT design. A point selection scheme is used to determine a small number of HSCT configurations which best describes the overall feasible design space. These HSCT configurations are then analyzed. This step in the procedure is the most time consuming and parallel computing can be efficiently used if available. The results of the analyses are used to generate response surface models using the method of least squares. The response surface models are then substituted into the optimization and a constrained optimization is performed. If the error between the response surface approximation and actual analysis at the final design is significant, the process is repeated by shrinking the boundaries of the design space around this final design, and computing response surface approximations within this new region.

6. Response Surface Approximation For Pitch-up and Flap Effect Parameters

In this study we apply response surface methodology to approximate the pitch-up and flap effect parameters ($C_{M\alpha,1}$, α_B, $C_{M\alpha,2}$, $\Delta C_{M\delta e}$, $\Delta C_{M\delta f}$, $\Delta C_{L\,\delta f}$) calculated by *Aero2s* and the APE method. The resulting response surface approximations will then be used within the optimization instead of directly calculating the above parameters using *Aero2s* and the APE method.

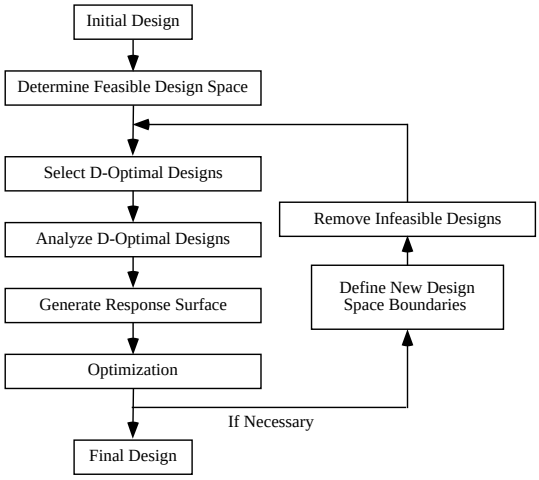

Figure 8. Response surface procedure.

6.1 Design Variable Selection

Nine of the 29 HSCT design variables (Table 1) were found to have an impact on the results calculated by the Aerodynamic Pitch-up Estimation (APE) method and therefore were used to develop the response surface models. These design variables included the horizontal tail and wing planform variables: wing root chord, wing tip chord, wing span, locations of the wing leading-edge and trailing-edge break points, and the location of the leading-edge of the wing tip (Figure 1). The remaining HSCT design variables were ignored in the development of the response surfaces.

6.2 Feasible Design Space

From a previous study[5], the reasonable design space was identified by constructing a large hypercube defined by varying three of the twenty-five geometric design variables (Table 1) at a time around the baseline design. This is known as a partially balanced incomplete block experimental design. A reasonable design refers to a design where all the geometric constraints are acceptable even though some of the aerodynamic and performance constraints are violated. Using this technique, 19,651 configurations were found on the boundary of the domain. A large percentage of these configurations violated one or more of the

HSCT's geometric constraints and therefore were unreasonable. Instead of eliminating unreasonable designs, a series of increasingly expensive criteria (Table 6) were used to move the candidate designs towards the reasonable design space. The final result is a series of candidate designs that surround the reasonable design space resulting in a more accurate response surface. The candidate designs for this study were chosen from the 19,651 points which were unique to this nine design variable pitching moment problem, resulting in 835 candidate design points. From these 835 candidate designs, a set of D-optimal set was selected. The actual size of the D-optimal designs was selected realizing that at least 55 designs are needed to solve a 55 coefficient, quadratic, nine variable response surface model, and that to obtain a good least squares fit about 2.5 times this number of designs is actually required. Thus, of the 835 candidate designs, 138 D-optimal designs were selected to generate the quadratic, nine variable response surface model.

Table 3. Criteria for reasonable designs (Ref. 5).

#	Description
1-34	HSCT geometric constraints (Table 2)
35-36	wing bending material > 20,000 lbs wing bending material < 120,000 lbs
37-58	Minimum fuselage radius
59	Inboard Λ_{le} > Outboard Λ_{le}
60	$\Lambda_{le} > 0$
61-62	5,000 sq. ft < wing area < 15,000 sq. ft
63-64	1.0 < aspect ratio < 3.2
65	Inboard $\Lambda_{te} < 40°$
66-83	$c_{y,i+1}/c_{y,i} < 1.0$
84	Approximate range > 5,000 n.mi.

6.3 Response Surface Generation

The above six parameters ($C_{M\alpha,1}$, α_B, $C_{M\alpha,2}$, $\Delta C_{M\delta e}$, $\Delta C_{M\delta f}$, $\Delta C_{L\,\delta f}$) were calculated for the D-optimal aircraft configurations. The resulting data were used to determine the coefficients of the response surface models for each of the six desired responses. After the generation of each response surface model, it was evaluated to determine how well it fit the actual data. A statistic known as the coefficient of multiple determination, or R^2 value, was used for this purpose (see the discussion at the end of Section 5.2). Table 4 lists the R^2, root mean square error, the mean of the response, and the number of observations (design evaluations) for each response surface model. The root mean square error estimates the standard deviation of the random error. The number of observations is the total number of design evaluations used in the fit.

As presented in Table 4, the response surface models for the pitching moment slope before pitch-up ($C_{M\alpha,1}$), slope after pitch-up ($C_{M\alpha,2}$), lift increment due to flap deflections ($\Delta C_{L\delta f}$) and the pitching moment increment due to flap deflections ($\Delta C_{M\delta f}$) fit the data very well since their R^2 values are all greater than 0.94, which is close to a perfect fit value of 1.0. The response surface models for the pitch-up angle-of-attack (α_B) and the pitching moment increment due to tail deflection ($\Delta C_{M\delta e}$) did not fit as well as the other response surface models, with R^2 values less than 0.90. This is attributed to noise or randomness in the data and to the nature of the unknown true response, which is not a true quadratic polynomial function of the design variables. Recall that the APE method does not actually compute a specific pitch-up angle of attack.

Table 4. Error estimates in the response surface models.

a. Pitching Moment

	$C_{M\alpha,1}$	α_B	$C_{M\alpha,2}$
R^2	0.989	0.881	0.950
Root mean square error	1.94e-4	0.931	3.32e-4
Mean of Response	-6.40e-4	7.622	2.31e-3
Observations	138	138	138

b. Control and Flap Effectiveness

	$\Delta C_{M\delta e}$	$\Delta C_{L\,\delta f}$	$\Delta C_{M\delta f}$
R^2	0.894	0.940	0.956
Root mean square error	9.64e-3	7.59e-3	3.49e-3
Mean of Response	6.89e-2	1.97e-1	-5.01e-2
Observations	138	138	138

7. HSCT Design Optimizations

Several HSCT design optimizations were performed with and without the response surface approximations for the pitch-up and flap effect parameters. These parameters were included within the analysis of the takeoff and landing constraints. The entire sequence of optimizations is presented in Figure 9. The baseline design shown at the top of the figure is used as a starting design for each optimization. This design is an HSCT configuration previously studied by Dudley *et al.*[4], but does not satisfy all of the constraints currently in our design problem. The optimizations labeled "without response surfaces" were completed using the original methods within the design code, which include a

linear relationship between pitching moment and angle-of-attack and the constant approximation of the flap effects. The remaining optimizations were performed with various response surface models substituted into the optimization process as listed in Table 5. In Case E, new response surface models were generated within a reduced design space around Case D and used during the optimization.

Table 5. List of response surface models used.

Case	$C_{M\alpha,1}$	α_B	$C_{M\alpha,2}$	$\Delta C_{M\delta_e}$	$\Delta C_{M\delta f}$	$\Delta C_{L\delta f}$
A						
B	✓					
C	✓	✓	✓			
D	✓	✓	✓	✓	✓	✓
E	✓	✓	✓	✓	✓	✓

Additional bounds on the design variables were added to the optimization to keep it within the response surface design space, along with a few other constraints as given in Table 6. The purpose was to reduce any exploitation of the response surface by the optimizer, which tries to move into regions where the response surface is invalid. From the values of the design variables for each D-optimal design, a minimum and maximum constraint value was established for each of the nine design variables listed in Table 6. Additionally, the geometrically reasonable design constraints of Table 3 were included in the optimization, except for the wing bending material weight constraints. Thus the total number of constraints increases from 69 to 111.

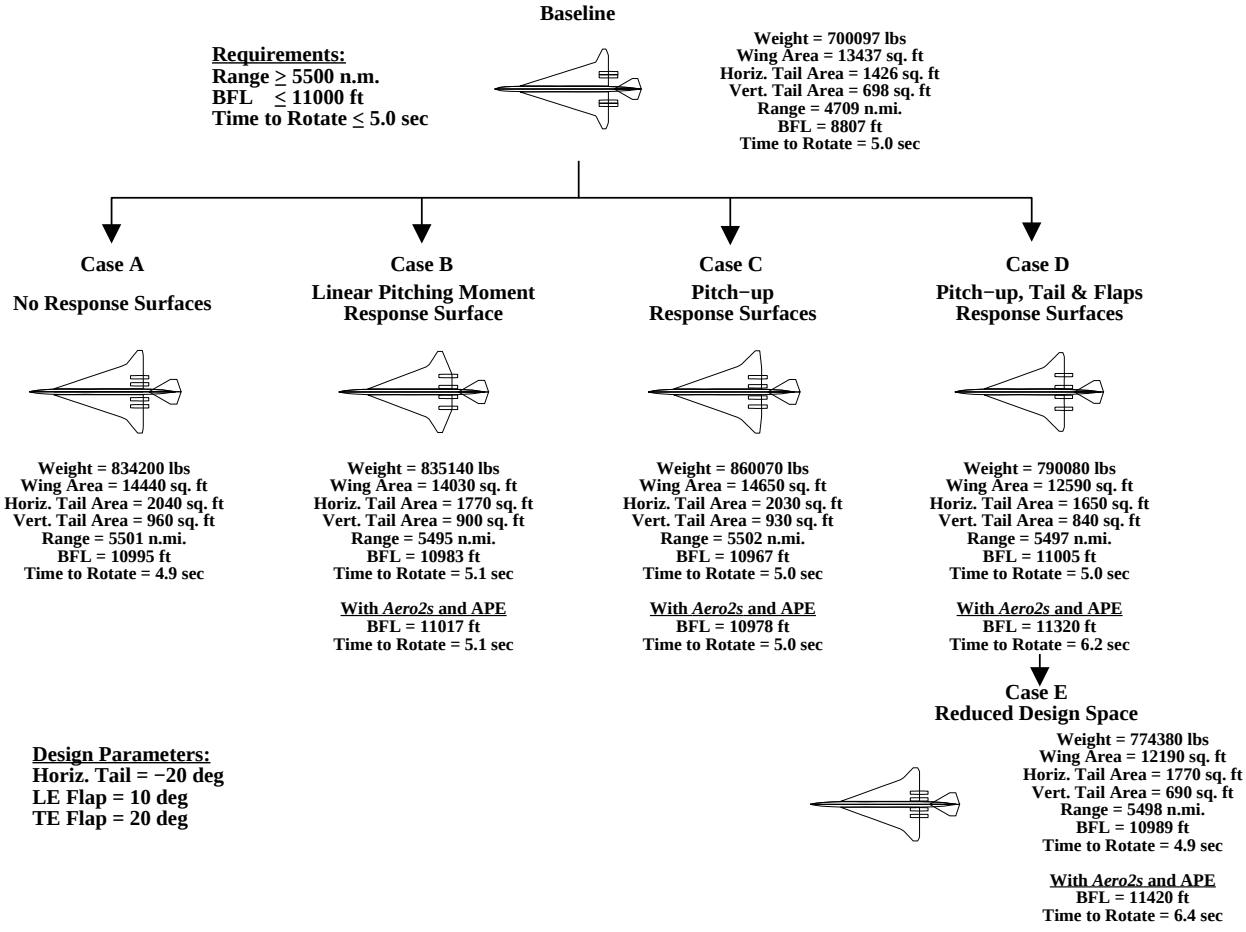

Figure 9. Series of HSCT optimization with and without response surfaces.

7.1 Case A

As previously mentioned, the baseline design did not satisfy all of the constraints in our current design problem. This optimization was performed to obtain an optimal design which satisfies the most recent modifications to the code by MacMillin[8] *et al*. without using response surface models. The initial baseline design shown at the top of Figure 9 has a TOGW of 700,097 *lbs* with a wing weight of 110,979 *lbs* and a fuel weight of 322,617 *lbs*. The range and balanced field length for this design were estimated at 4,709 *n. mi.* and 8807 *feet* respectively.

The initial baseline design violated the range constraint, two thrust constraints, the takeoff rotation constraint, nacelle spacing constraint, and the engine out stability constraint. After 27 optimization cycles, the final design increased 134,000 *lbs* to a final TOGW of 834,000 *lbs* with all the constraints satisfied. Since the most heavily weighted constraint was the range constraint, the wing area increased 1,000 ft^2 with an additional wing weight of 22,100 *lbs*, the fuel increased 106,400 *lbs*, and the lift-to-drag ratio (*L/D*) increased from 9.1 to 9.4 to obtain the required mission range of 5,500 *n. mi.* In addition, the vertical tail size increased 260 ft^2 to satisfy the engine out stability requirement. The horizontal tail size increased 620 ft^2 to satisfy the balanced field length and time-to-rotate constraints. The inboard engine also moved inboard to satisfy the nacelle spacing constraint. For Case A the balanced field length was 10995 ft and the time to rotate was 5.0 sec.

7.2 Case B

This optimization substituted the pitching moment curve slope ($C_{M\alpha}$) into the linear relationship of the pitching moment with angle-of-attack and was not calculated by the aerodynamic models within the design code. Since a response surface model was included, the number of constraints was increased from 69 to 111. The same initial design is used in this optimization. After 50 optimization cycles, the TOGW increased slightly to 835,100 *lbs* with all the constraints satisfied.

As shown in Figure 9, this optimal design has an unusual planform with a forward swept trailing-edge. The driving constraints for this problem were the engine-out stability constraint and the two thrust constraints. During this optimization, the wing trailing-edge break location moved inboard and the leading-edge wing tip moved forward to decrease the wing weight and overall TOGW. Since we are solving for a minimum weight design, the optimizer chose to decrease the TOGW by designing a lighter wing instead of increasing the size of the engines, which would increase the weight, to satisfy the thrust constraints.

Using the single response surface for $C_{M\alpha}$, the optimal HSCT configuration had a balanced field length of 10983 ft and a time to rotate of 5.1 sec. For comparison, the *Aero2s* and APE methods were used to calculate the actual balanced field length and time to rotate which were 11017 ft and 5.1 sec, respectively. Although the error in the balanced field length was only 0.31 percent, the increase would violate the balanced field length constraint.

7.3 Case C

This optimization included the response surface models for pitch-up: the pitching moment slope before pitch-up ($C_{M\alpha,1}$), pitch-up angle-of-attack (α_B), and slope after pitch-up ($C_{M\alpha,2}$). The same initial design was used in this optimization. After 45 optimization cycles, the TOGW increased to 860,100 *lbs* with all the constraints satisfied.

This optimal design is the heaviest at a TOGW of 860,100 *lbs*. The driving constraints for this problem were also the engine-out stability constraint and the two thrust constraints. However, the trailing-edge is not swept forward as in the previous case. Since the trailing-edge is not swept forward, the wing is 11,300 *lbs* heavier than the wing in Case B. In addition, the design also carries heavier engines and a larger vertical and horizontal tail to control the heavier aircraft. There are two possible explanations for the differences in the design. The first and simplest is that the design may be stuck in a local minimum. A more complex explanation may be that sweeping the trailing-edge forward has a great affect on pitch-up.

With the response surface models for $C_{M\alpha,1}$, α_B, and $C_{M\alpha,2}$ the balanced field length was 10967 ft and the time to rotate was 5.0 sec. Using the *Aero2s* and APE methods, the actual balanced field length was 10978 ft and the actual time to rotate was 5.0 sec. For this case, the error in balanced field length was 0.10 percent and the balanced field length constraint would remain satisfied.

Figure 10 presents the pitch-up angle-of-attack during the design history of Case B and C. As shown in the figure, the designs during the optimization of Case B drive towards a very low pitch-up angle-of-attack (α_B) around 3 degrees, while the designs during the optimization of Case C all have pitch-up angles-of-attack around 7 degrees. Keep in mind that the optimization of Case B did not include pitch-up and ignored the pitch-up angle-of-attack information which may have affected the results.

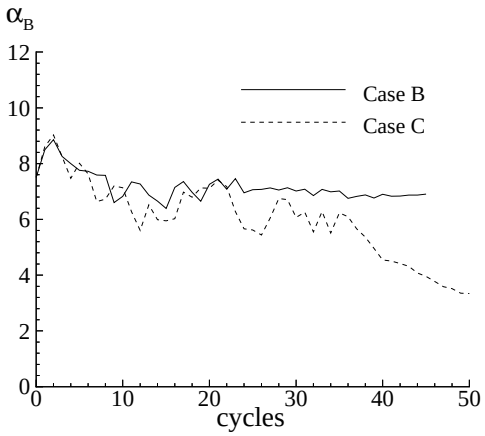

Figure 10. Response surface values throughout the optimization history of Case B and C.

7.4 Case D

The final two optimizations included response surface models for the increment in pitching moment due to tail deflection ($\Delta C_{M\delta e}$) and the increment in lift and pitching moment due to flap deflections ($\Delta C_{L\,\delta f}$, $\Delta C_{M\delta f}$) which are not held constant in this optimization. The pitch-up response surface models ($C_{M\alpha,1}$, α_B, $C_{M\alpha,2}$) were also included. The same initial design is used in this optimization. After 38 optimization cycles, the TOGW increased to 790,100 *lbs* with all the constraints satisfied.

This optimal design is considerably smaller and lighter than the previous optimal designs. The final weight is close to 70,000 *lbs* lighter than the previous optimization. In addition, the wing planform, horizontal tail, and vertical tail sizes are 2060 ft^2, 380 ft^2 and 90 ft^2 smaller respectively. The reason for this lightweight design is the difference between the pitching moment values predicted by the response surface models and the values which would have been calculated by the original design code. As shown in Figure 11, the increment in lift due to flap deflection calculated by the response surface model is over twice the constant value set during the previous optimizations. In addition, the increment in pitching moment due to elevator deflection is calculated 0.02 greater than the value calculated by JKayVLM. The increment in pitching moment due to flap deflection is calculated as 0.013 less than the constant value set during the other optimizations. Therefore, for a given design, the balanced field length and time-to-rotate would be shorter using the response surface approximations. As a result, the design can be designed with a smaller wing planform and smaller control surfaces to achieve the same performance.

Using *Aero2s* and APE, the actual pitching moment was calculated and the takeoff and landing constraints were recalculated. Using actual pitching moment data, the balance field length increased to 11,320 *ft* and the time to rotate increased to 6.2 *sec*, which now violate the constraints of 11,000 *ft* and 5.0 *sec* respectively.

The accuracy of the response surface approximations throughout the optimization was investigated and presented in Figure 12. This figure compares the response surface values for each parameter to the "actual" values calculated by *Aero2s* and the APE method throughout the history of the optimization. As presented, the parameters calculated by the response surface were relatively accurate near the beginning of the optimization and increased in error as the optimization progressed. This trend was expected since a quadratic polynomial response surface was generated around the initial design point and the error bounds increase as the design moves further away from the initial design. As shown in the figure, the final value of each parameter was predicted reasonably well using the response surface models, except for the pitching moment increment due to tail deflection ($\Delta C_{M\delta e}$) which was over-predicted approximately 28% of the actual value. This would explain the large increase in balance field length and time to rotate. The optimizer believed it had more control power from the horizontal tail than it actually did.

7.5 Case E

To investigate the possibility of improving the predicted response of the response surface models, a factorial design of experiment was generated over a smaller design space surrounding a design point of interest instead of approximating the response surface over the entire feasible design space. The design point of interest was chosen as the optimal configuration of Case D and the design variables were allowed to vary as specified in Table 6.

Simple geometric constraints were used to screen out 12,150 infeasible geometric designs out of 19,683 three-level nine-variable factorial designs. In this case, the infeasible designs were thrown out instead of moving the designs towards the feasible geometric design space. New response surfaces were generated using 150 D-optimal points of the remaining *feasible* factorial designs and Table 7 lists their corresponding R^2 value. As shown in the table, the response surfaces predicted the true response very well except for the pitch-up angle of attack response surface model. The poor response in the pitch-up angle-of-attack is due to the fact that several of the D-optimal configurations exhibited a linear pitching moment curve throughout the entire angle-of-attack regime. With our assumptions that pitch-up must occur, the specific angle of attack at which pitch-up occurred

was not easily identified within the data and therefore there were large fluctuations in the prediction.

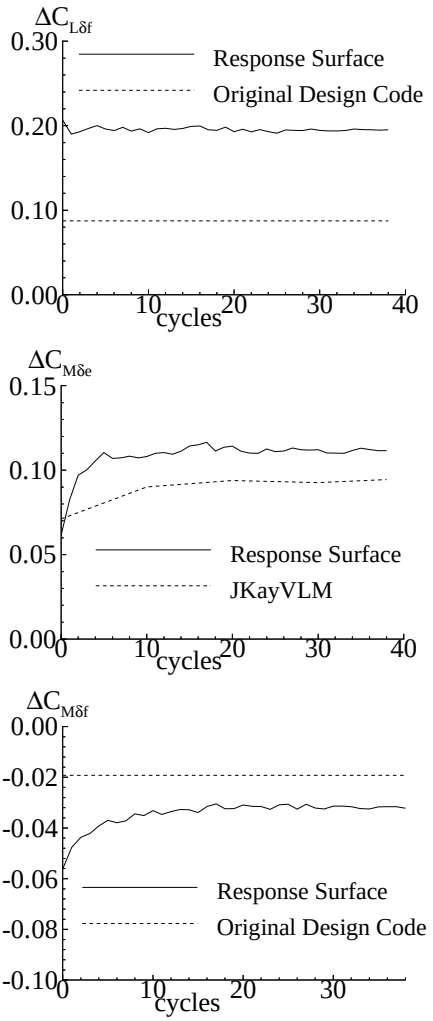

Figure 11. Response surface values vs. design code values.

Using the "improved" response surfaces, the final optimal configuration (Case E) is shown in Figure 9. The final result has a wing planform similar to Case D. The takeoff gross weight decreased 15,700 *lbs*. The vertical tail decreased in size since the engines were allowed to move inboard. The horizontal tail size increased since the initial balanced field length was 11,350 *ft*.

Using *Aero2s* and APE, the actual pitching moment was calculated and the takeoff and landing constraints were recalculated. Using actual pitching moment data, the balance field length increased to 11,420 *ft* and the time to rotate increased to 6.4 *sec*, which still violate the constraints of 11,000 *ft* and 5.0 *sec* respectively.

As in the previous case, the accuracy of the response surface approximations throughout the optimization was investigated and is presented in Figure 13. In this case, each parameter was reasonably predicted by the response surface models, except for the pitch-up angle of attack (α_B) and the pitching moment due to tail deflection ($\Delta C_{M\delta e}$). The fluctuation in pitch-up angle of attack is due to the difficulty in calculating the angle-of-attack at which pitch-up occurs among near-linear data. The final value of $\Delta C_{M\delta e}$ was overpredicted by 24 percent and the result is the large difference in balanced field length and time to rotate.

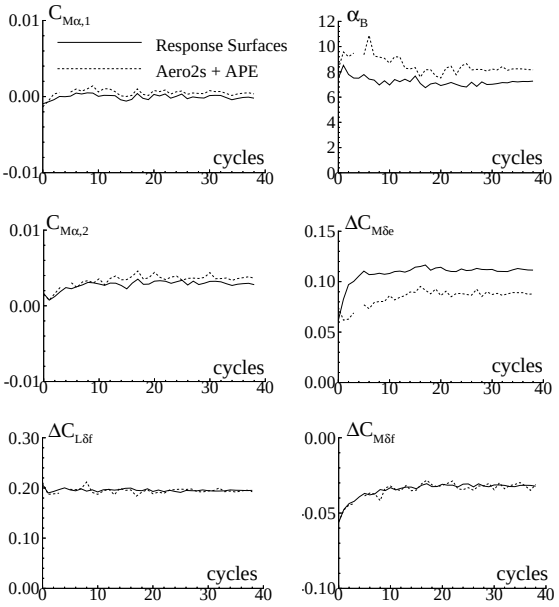

Figure 12. Response surface values vs. actual response (Case D).

Table 6. Factorial design limits.

Design Variables	Baseline Value	Variation	
root chord, ft.	164.5	-10%	+10%
x-location of the LE break, ft.	123.7	-10%	+10%
y-location of the LE break, ft.	43.9	-10%	+10%
x-location of the TE break, ft.	164.5	-10%	+10%
y-location of the TE break, ft.	66.3	-10%	+10%
x-location of the wing tip LE, ft.	154.2	-10%	+10%
wing tip chord, ft.	7.4	-0%	+50%
wing semi-span, ft.	73.7	-10%	+10%
horizontal tail area, ft^2	827.4	-30%	+30%

Table 7. Response surface fit over reduced design space for Case D.

a. Pitching moment

	$C_{M\alpha,1}$	α_B	$C_{M\alpha,2}$
R^2	0.992	0.684	0.929
Root mean square error	1.65e-4	1.30	4.61-4
Mean of Response	1.00-3	6.91	3.99e-3
Observations	150	150	150

b. Control and Flap Effectiveness

	$\Delta C_{M\delta e}$	$\Delta C_{L\,\delta f}$	$\Delta C_{M\delta f}$
R^2	0.974	0.954	0.982
Root mean square error	6.75e-3	5.67e-3	2.83e-2
Mean of Response	8.40e-2	1.94e-1	-3.54e-2
Observations	150	150	150

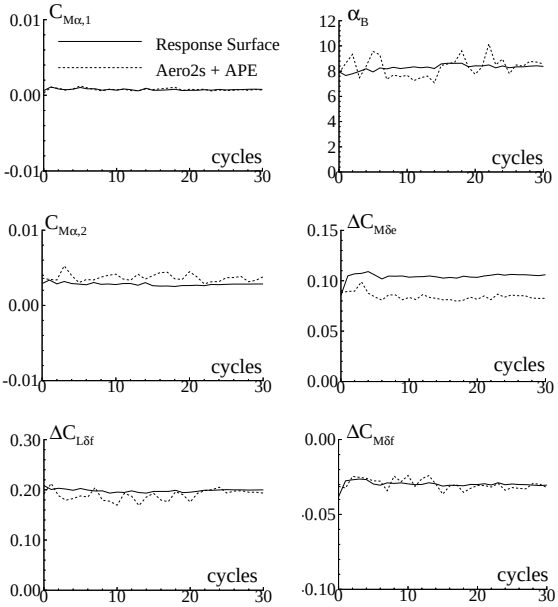

Figure 13. Response surface values vs. actual response (Case E).

8. Conclusions

The objective of this project was to develop a procedure to incorporate nonlinear aerodynamics including pitch-up and to develop an improved model to estimate the lift and moment flap effects within the multidisciplinary design optimization of a high-speed civil transport and to study their effect on the design. A vortex lattice code, *Aero2s*, and the Aerodynamic Pitch-up Estimation (APE) method were used to develop a nonlinear pitching moment model including pitch-up and to model flap effects. Since an analysis by *Aero2s* and the APE method takes several minutes and many analyses are needed to incorporate the nonlinear pitching moment and flap effect models within the optimization, response surface methodology was used to approximate the results from *Aero2s* and the APE method by developing polynomial approximations (or response surfaces) through selected data collected prior to the optimization. Optimizations were completed with and without these polynomial approximations. A summary of the optimizations is listed in Table 8.

Table 8. Summary of optimizations.

Case	Idea	TOGW (lbs)
	Initial design	700,000
A	No response surfaces	834,200
B	Linear C_M response surface	835,140
C	Pitch-up response surfaces	860,070
D	All response surfaces	790,080
E	Reduced design space	774,380

In conclusion, this project demonstrated a way to incorporate nonlinear aerodynamics into the design optimization and did find that pitch-up had an effect on the aircraft design. Response surfaces were used to include pitch-up and flap effects into the optimization and were found to be a useful tool. Although errors in the response surface approximation can affect the final output of the optimization, and we are continually developing refinements, this approach to incorporation of nonlinear aerodynamics is a key to a practical MDO methodology for complex nonlinear systems.

9. Acknowledgments

This work was supported under the NASA/Universities Space Research Association Advanced Design Program, with Peter Coen of NASA Langley as the Center Mentor. We gratefully acknowledge this support.

10. References

1. McCullers, L. A., "Aircraft Configuration Optimization Including Optimized Flight Profiles," *Proceedings of a Symposium on Recent Experiences in Multidisciplinary Analysis and Optimization*, J. Sobieski, compiler, NASA CP-2327, Apr. 1984, pp. 395-412.

2. Jayaram, S., Myklebust, A., and Gelhausen, P., "ACSYNT - A Standards-Based System for

Parametric, Computer Aided Conceptual Design of Aircraft," AIAA Paper 92-1268, Feb. 1992.

3. Hutchison, M. G., Unger, E. R., Mason, W. H., Grossman, B., and Haftka, R. T., "Variable-Complexity Aerodynamic Optimization of an HSCT Wing Using Structural Wing-Weight Equations," *Journal of Aircraft*, Vol. 31, No. 1, 1994, pp. 110 -116.

4. Dudley, J., Huang, X., Haftka, R. T., Grossman, B., and Mason, W. H., "Variable-Complexity Interlacing of Weight Equation and Structural Optimization for the Design of the High Speed Civil Transport," AIAA Paper 94-4377, 1994.

5. Kaufman, M., Balabanov, V., Burgee, S., Giunta, A. A., Grossman, B., Mason, W. H., Watson, L. T., and Haftka, R. T., "Variable-Complexity Response Surface Approximations for Wing Structural Weight in HSCT Design," 34th Aerospace Sciences Meeting and Exhibit, AIAA Paper 96-0089, Reno, NV, Jan. 1996.

6. Giunta, A. A., Narducci, R., Burgee, S., Grossman, B., Mason, W. H., Watson, L. T., and Haftka, R. T., "Variable-Complexity Response Surface Aerodynamic Design of an HSCT Wing," *Proceedings of the 13th AIAA Applied Aerodynamics Conference*, AIAA Paper 95-1886, pp. 994-1002, San Diego, CA, June 19-22, 1995.

7. Benoliel, A. M. and Mason, W. H., "Pitch-up Characteristics for HSCT Class Planforms: Survey and Estimation," AIAA 12th Applied Aerodynamics Conference, AIAA Paper 94-1819, Colorado Springs, CO, June 1994.

8. MacMillin, P. E., Golividov, O., Mason, W.H. Grossman, B., and Haftka, R.T., "Trim, Control, and Performance Effects in Variable-Complexity High-Speed Civil Transport Design," MAD Center Report 96-07-01, July 1996. Virginia Tech, Blacksburg, VA: http://www.aoe.vt.edu/mad/reports

9. Grandhi, R. V., Thareja, R., and Haftka, R. T., "NEWSUMT-A: A General Purpose Program for Constrained Optimization Using Approximations," *ASME J. Mechanisms, Transmissions and Automation in Design*, Vol. 107, 1985, pp. 94-99.

10. Hutchison, M. G., *Multidisciplinary Optimization of High-Speed Civil Transport Configurations Using Variable-Complexity Modeling*. PhD Thesis, Virginia Polytechnic Institute & State University, Blacksburg, Virginia, Mar. 1993.

11. Hoak, D. E., *et al.*, *USAF Stability and Control DATCOM*. Flight Control Division, Air Force Flight Dynamics Laboratory, WPAFB, Ohio, 45433-00001, 1978. Revised.

12. Antani, D. L. and Morgenstern, J. M., "HSCT High-Lift Aerodynamic Technology Requirements," AIAA Paper 92-4228, Aug. 1992.

13. Kay, J., Mason, W. H., Durham, W., and Lutze, F., "Control Authority Assessment in Aircraft Conceptual Design," AIAA Paper 93-3968, Aug. 1993.

14. Baber, Jr., H. T., "Characteristics of the Advanced Supersonic Technology AST-105-1 Configured for Transpacific Range with Pratt and Whitney Aircraft Variable Stream Control Engines," NASA TM-78818, March 1979.

15. Wright, B.R., Bruckman, F., and Radovich, N.A., "Arrow Wings for Supersonic Cruise Aircraft," *Journal of Aircraft*, Vol. 15, No. 12, pp. 829-836, December 3, 1978.

16. Carlson, H. W., Darden, C. M., and Mann, M. J., "Validation of a Computer Code for Analysis of Subsonic Aerodynamic Performance of Wings With Flaps in Combination With a Canard or Horizontal Tail and an Application to Optimization," NASA TP-2961, 1990.

17. Yip, Long P. and Lysle P. Parlett. "Low-Speed Wind-Tunnel Tests of a 1/10-Scale Model of an Arrow-Wing Supersonic Cruise Configuration Designed for Cruise at Mach 2.2," NASA TM-80152, 1979.

18. Quinto, P. F. and John W. P., "Flap Effectiveness on Subsonic Longitudinal Aerodynamic Characteristics of a Modified Arrow Wing," NASA TM-84582, 1983.

19. Myers, R. H. and Montgomery, D. C., *Response Surface Methodology: Process and Product Optimization Using Designed Experiments*, John Wiley & Sons, Inc., 1995.

20. Mason, R. L., Gunst, R. F., and Hess, J. L., *Statistical Design and Analysis of Experiments*, John Wiley & Sons, New York, N. Y., 1989, pp. 215-221.

21. Box, M. J. and Draper, N. R., "Factorial Designs, the $|\mathbf{X}^T\mathbf{X}|$ Criterion, and Some Related Matters," *Technometrics*, Vol. 2, No. 4, Nov., 1960, pp. 455-475.

22. Giunta, A. A., Dudley, J. M., Narducci, R., Grossman, B., Haftka, R. T., Mason, W. H., and Watson, L. T., "Noisy Aerodynamic Response and Smooth Approximations in HSCT Design," Proceedings of the 5th AIAA/USAF/NASA/ISSMO Symposium on Multidisciplinary Analysis and Optimization, AIAA Paper 94-4376, Panama City Beach, FL, Sept. 1994, pp. 1117-1128.